DOI: 10.37990/medr.1305549 Med Records 2023;5(3):507-12

MEDICAL RECORDS-International Medical Journal

Research Article

Quantitative Assessment of the Pharyngeal Recess Morphometry in Anatolian Population Using 3D Models Generated from Multidetector Computed Tomography Images

Huseyin Erdem[1], Mustafa Tekeli[1], Yigit Cevik[1], Nazire Kilic Safak[1], Omer Kaya[2], Neslihan Boyan[1], Ozkan Oguz[1]

[1] Cukurova University, Faculty of Medicine, Department of Anatomy, Adana, Türkiye
[2] Cukurova University, Faculty of Medicine, Department of Radiology, Adana, Türkiye

Abstract

Aim: It was aimed to analyze the detailed morphometry of the pharyngeal recess (PR) using three-dimensional (3D) models reconstructed from multidetector computed tomography (MDCT) images.

Material and Methods: This study was a retrospective analysis and performed on MDCT images of 97 patients (43 males, 54 females). 3D models of the PR were reconstructed using 3D Slicer software, enabling morphometric measurements according to established protocols. Measurements included PR depths, distances between the posterior nasal spine and torus levatorius (PNS-TL), distances between right and left TL (RTL-LTL) distances between the PNS and posterior wall of the nasopharynx (PNS-PWN), the angle (α) between the centerline of the PR and the sagittal plane. The morphologies of the PR classified into three types.

Results: The average measurements for the parameters were as follows: PR depth - 10.42 mm, distance between PNS and TL - 10.40 mm, distance between RTL and LTL - 19.13 mm, distance between PNS and PWN - 19.92 mm, and the angle (α) - 53.65°. The prevalence of PR types was 20.62%, 47.42% and 31.96% for type 1, type 2 and type 3, respectively.

Conclusion: Variations in reported measurements of the pharyngeal recess can be attributed to imaging techniques, patient positioning, anatomical differences, and sample sizes. The use of 3D models generated from MDCT datasets offers a high-resolution and comprehensive approach to understanding the PR's morphometry and spatial relationships, enabling accurate measurements and advancing our knowledge of this anatomical region.

Keywords: 3D slicer, multidetector computed tomography, nasopharyngeal carcinoma, nasopharynx, pharyngeal recess

INTRODUCTION

The pharyngeal recess (PR), also referred to as the Rosenmüller fossa, is a well-known anatomical structure that is bilaterally located in the nasopharynx, below the skull base (1). The eponymously attributed nomenclature of the PR originates from its first description in 1808 by Johann Christian Rosenmüller, a German anatomist (2). Although it is a relatively small area in the aerodigestive tract, it is clinically important as it is an anatomical region where nasopharyngeal carcinoma (NPC) malignancies originate (3).

The PR is formed by the nasopharyngeal mucosal reflection over the longus colli and surrounded by distinct anatomical structures. The eustachian tube and levator veli palatini demarcate its anterior boundary, while the posterior wall of the nasopharynx and retropharyngeal space limits posteromedialy. Laterally, the fossa is bordered by the parapharyngeal space and tensor veli palatini, also the superior border of the constrictor superior marks its inferior extent. The skull base constitutes the superior boundary of this fossa. Furthermore it is in close proximity to the internal carotid artery through its roof (4-6).

Since the primary diagnostic evidence for the NPC is asymmetry and blunting in the PR, utilization of innovative 3D imaging modalities are essential for the detailed evaluation of the area (7). The superior spatial resolution and image quality offered by MDCT, render it an

CITATION
Erdem H, Tekeli M, Cevik Y, et al. Quantitative Assessment of the Pharyngeal Recess Morphometry in Anatolian Population Using 3D Models Generated from Multidetector Computed Tomography Images. Med Records. 2023;5(3):507-12. DOI:1037990/medr.1305549

Received: 19.05.2023 **Accepted:** 09.06.2023 **Published:** 13.07.2023
Corresponding Author: Huseyin Erdem, Cukurova University, Faculty of Medicine, Department of Anatomy, Adana, Türkiye
E-mail: herdem@cu.edu.tr

indispensable tool for exploring the PR morphology and ultimately diagnosing the NPC (8). However, the spatial localization in bilateral symmetry of the structures that compose the PR or adjacent structures are typically not congruent within the same axial plane, thus hindering the accuracy of morphometric assessments (9). The rotational functionality provided by radiological visualization software tools may potentially address this issue by revolving the entire Digital Imaging and Communications in Medicine (DICOM) dataset around specific landmarks following the creation of three-dimensional (3D) reconstructions. Nonetheless, this recourse may not be feasible due to the absence of such tools in frequently utilized stationary software. Third-party software, which facilitate the creation of 3D reconstructions from DICOM datasets, offer the added advantage of rotational movement of radiological planes or models, thereby enabling the execution of precise morphometric analysis (10).

The diagnosis of NPC conventionally relies on the utilization of ear, nose, and throat (ENT) clinical evaluation methods, where the MRI and MDCT images acquired in the supine position are employed by ENT specialists to achieve accurate diagnosis (11). Therefore, to analyze the morphometric features of the PR, 3D digital models were reconstructed in this study using DICOM datasets of the MDCT images obtained from patients in the supine position. It was aimed to enhance the current knowledge about this crucial anatomical region, thereby facilitating diagnosis and treatment of the NPC.

MATERIAL AND METHOD

This retrospective study received approval from the local non-interventional clinical research ethics committee (Protocol no: 7.4.23/132) and adhered to the principles outlined in the Declaration of Helsinki. The dataset for this study consisted of axial MDCT images of patients screened between January 2022 and December 2022. A randomized approach was employed to select MDCT images from the archive of the Radiology Department at the Faculty of Medicine, Cukurova University. The scans were conducted using a 160-slice MDCT scanner (Toshiba Aquilion™ PRIME; Otawara, Japan) with a standard protocol of 0.6 mm collimation, 0.5 mm slice thickness, 120 kV, and 250 m. A bone window setting (Width: 2500; Level: 500) and a digital workstation (Vitrea CT workstation, Toshiba; Otawara, Japan) were used to evaluate the images. A series of 171 MDCT images from supine patients, with their head and neck in neutral position and the Frankfort horizontal plane perpendicular to the floor, were selected. After applying exclusion criteria (trauma, tumors, incomplete images, swellings or malformation of the nasopharyngeal region) 97 MDCT images were remained and anonymized. The DICOM datasets of those patients were used in the study.

Segmentation of the 3D models was carried out utilizing *3D Slicer*. In the *Segment Editor Module* thresholding was manually adjusted for the segmentation of 3D models. Two distinct segmentations were conducted: one for the bones (yellow) and the other for the soft tissue (green). The resultant 3D models of both bones and soft tissue were then merged in the same workspace. To facilitate further morphometric analysis, the anatomical landmarks were designated using the *Paint Tool*. The axial MDCT plane was manually scrolled and subsequently rotated within the x, y, z coordinates, until proper alignment was achieved with the identified anatomical landmarks (Figure 1). The sagittal plane was scrolled laterally until the bilateral components of the PR became visible. The 3D models cropped through the determined axial and sagittal planes (Figure 2) and morphometric measurements were performed in the *Markups Module.*

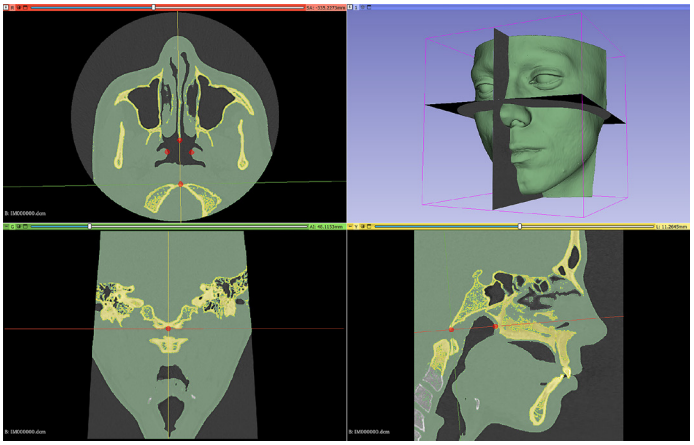

Figure 1. Landmarks were determined on axial planes (red dots). The axial plane aligned through the basion + PNS and Right PR + Left PR. The sagittal plane was aligned through the basion and PNS

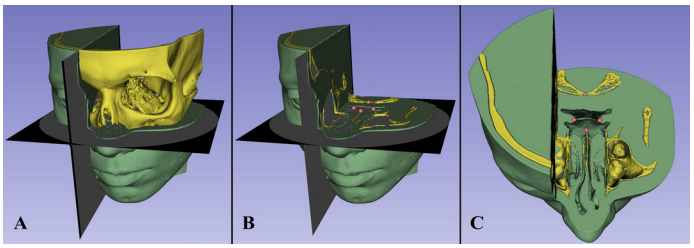

Figure 2. The sagittal plane scrolled through the lateral side (right side) until whole PR structures were viewed. Soft tissue **(A)** and the skull **(B)** were cut-out from the intersection of the planes to visualize the landmarks **(C)**

Following the identification of the relevant landmarks, morphometric measurements were carried out in accordance with established protocols (Figure 3). The distances and angles were measured three times, averaged, and the resulting mean value documented as the final value:

LPR Depth: Vertical distance to the line connecting LTL (c) with basion (d)
RPR Depth: Vertical distance to the line connecting RTL (b) with basion (d)
a-e: Distance between PNS and PWN
f-b: Distance between PNS and RTL
g-c: Distance between PNS and LTL
b-c: Distance between RTL and LTL
RPRα: The angle between the centerline of the RPR and

the sagittal plane
LPRα: The angle between the centerline of the LPR and the sagittal plane

The morphologies of the PRs were initially classified into three types: Type 1 (fossa depth <5 mm), Type 2 (fossa depth ≥ 5 mm and opening width <1 mm), and Type 3 (fossa depth ≥ 5 mm and opening width ≥1 mm).

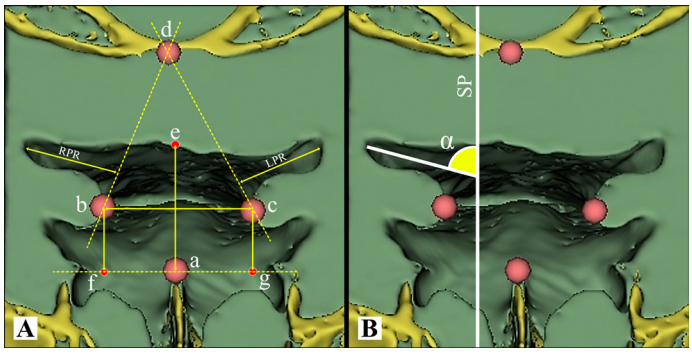

Figure 3. A. Distances were measured through the determined landmarks on finalized 3D models. **a.** Posterior nasal spine (PNS); **b.** Right torus levatorius (RTL); **c.** Left torus levatorius (LTL); **d.** Basion; **e.** Posterior wall of the nasopharynx (PWN); **f.** Projection of the RTL on the horizontal line passing through the PNS; **g.** Projection of the LTL on the horizontal line passing through the PNS. Additionally, a horizontal line passing through the PNS, and also lines connecting RTL (b) and LTL (c) with basion (e) was generated. **B. α.** The angle between the centerline of the PR and the sagittal plane (the angle of the right pharyngeal recess-RPRα was shown for representative purpose on the figure). SP: sagittal plane

Statistical Analysis

Data were analyzed using IBM SPSS Statistics Version 20.0 statistical software package (SPSS Inc., Chicago, IL, USA). Continuous variables were summarized as mean and standard deviation and as median and minimum-maximum. The Kolmogorov–Smirnov test was employed to classify the distribution of the datasets into parametric and nonparametric data. The Mann-Whitney U test was used to compare the morphometric variables between male and female groups, while Spearman's r correlation was used to examine the relationship between variables. The Wilcoxon rank-sum test was used to analyze TL, PR, and angle parameters on both sides. The frequencies of PR types were compared by gender using a chi-square test for significance. Inter-observer reliability analysis was performed on measurements taken by two observers, with the primary observer (HE) conducting the initial measurements and the secondary observer (MT) conducting the same measurements while being blinded to the initial measurements. Intraclass correlation coefficients (ICC) were utilized to evaluate the level of agreement between the two observers and assess inter-observer reliability. The statistical level of significance for all tests was considered to be 0.05.

RESULTS

The ICC values for each of the measurements are presented in (Table 1), indicating good to excellent inter-observer reliability, as per the evaluation of Koo and Li (2016) (12).

In this study, the DICOM datasets of 97 patients (43 males and 54 females) were analyzed. The average age of the patients was 50.77±16.72 years with a range of 22-81 years. The mean age for males and females were 54.00±15.86 years and 48.20±17.09 years, respectively. There was no significant difference observed in the age and other parameters between males and females (Table 2). The Wilcoxon rank-sum test revealed no significant differences for TL (p = 0.077) and PR (p = 0.059), but a significant difference for angle (p = 0.010). A strong positive correlation was observed between the left and right depths of the PR (Table 3). Moreover, a very strong positive correlation was found between the lengths of the TL and the depths of the PR in the same sides (Table 3).

The PR type data indicate a higher prevalence of type 2, with a frequency of 46% in males and 58.7% in females. Conversely, type 1 morphology was less common, representing 26.5% of males and 21.3% of females. Type 3 prevalence rate was 27.5% in males and 30% in females.

Table 1. Intra-observer reproducibility and reliability for each the measurements taken

Parameters	ICC (95% CI)	p
Left PR	0.933 (0.829-0.973)	<0.001
Right PR	0.921 (0.800-0.969)	<0.001
Left TL	0.860 (0.647-0.945)	<0.001
Right TL	0.871 (0.674-0.949)	<0.001
Left TL – Right TL	0.908 (0.767-0.963)	<0.001
PNS – PWN	0.928 (0.818-0.972)	<0.001
Left Angle	0.894 (0.733-0.958)	<0.001
Right Angle	0.880 (0.696-0.952)	<0.001
Type Left	0.966 (0.922-0.988)	<0.001
Type Right	0.929 (0.820-0.972)	<0.001

ICC: intraclass correlation coefficient CI: confidence interval

Table 2. Distribution of male and female morphometric measurements

Parameters	n	Total	Male	Female	p
Age	97	50.77±16.72 54.00 (22.00-81.00)	54.00±15.86 60.00 (22.00-81.00)	48.20±17.09 48.00 (22.00-78.00)	0.084
PR (mm)	97	10.42±4.35 11.50 (1.97-19.27)	10.00±5.25 11.24 (1.97-19.27)	10.76±3.49 11.56 (2.31-18.04)	0.791
PNS-TL (mm)	97	10.40±4.39 11.40 (1.89-19.27)	9.88±5.33 11.24 (1.89-19.45)	10.82±3.46 11.48 (2.18-18.04)	0.594
RTL – LTL (mm)	97	19.13±3.49 19.17 (11.97-29.61)	19.00±4.02 18.82 (11.97-29.61)	19.13±3.05 19.21 (14.03-26.78)	0.862
PNS – PWN (mm)	97	19.92±3.43 20.10 (10.03-28.45)	20.03±3.06 20.70 (10.03-24.67)	19.84±3.73 19.07 (12.49-28.45)	0.396
Angle (α) (°)	97	53.65±6.94 53.41 (39.92-72.96)	53.49±7.08 53.47 (39.92-67.03)	53.79±6.90 53.33 (41.10-72.96)	0.994
PR Types n (%)	Type 1	40 (20.62%)	23 (26.74%)	17 (15.74%)	0.169
	Type 2	92 (47.42%)	38 (44.19%)	54 (50%)	
	Type 3	62 (31.96%)	25 (29.07%)	37 (34.26%)	

Values are given as Mean±Standard Deviation and Median (Min-Max)

Table 3. Spearman correlation coefficients (r) between pairs of parameters for each side and between the left and right sides

	Age	LPR	RPR	PNS-LTL	PNS-RTL	RTL-LTL	PNS-PWN	Left α
LPR	-0.122							
PPR	-0.096	0.742**						
PNS-LTL	-0.102	0.971**	0.757**					
PNS-RTL	-0.090	0.760**	0.978**	0.775**				
RTL-LTL	-0.035	0.376**	0.347**	0.335**	0.340**			
PNS-PWN	0.281**	0.154	0.178	0.159	0.173	0.191		
Left α	-0.072	0.015	-0.197	0.036	-0.222*	-0.201*	-0.028	
Right α	-0.086	0.008	-0.136	0.041	-0.132	-0.143	0.170	0.602**

**. Correlation is significant at the 0.01 level (2-tailed)
*. Correlation is significant at the 0.05 level (2-tailed)

DISCUSSION

In this study, 3D head models generated from DICOM datasets were used. It was aimed to enhance the reproducibility of the measurements by employing accurate and clear landmarks. The utilization of reconstructed 3D models provided a comprehensive understanding of the spatial relationships between anatomical structures within the nasopharynx. These measurements carry significant implications for surgical planning, radiation therapy, and the diagnosis of various pathologies in this region. Despite substantial advancements in medical knowledge concerning the anatomy of the PR, it remains an area of paramount clinical importance due to its high prevalence in the occurrence of NPC. Early detection of NPC is essential for timely treatment, which in turn contributes to improved survival rates (13).

Cone beam computed tomography (CBCT) imaging plays a crucial role in providing detailed three-dimensional information, enabling accurate diagnosis and treatment planning in various dental applications (14). In addition, it is also more practical and less time-consuming in terms of scanning patients in the upright position (15). Sutthiprapaporn et al. (2008) highlighted the advantage

of upright positioning during CBCT scans to minimize gravitational effects that may distort PR morphology typically observed in supine MDCT imaging (16). They also stated that CBCT imaging may facilitate the early diagnosis of NPC (9). In our analysis of radiology archive images, we identified cases with distorted PR morphology, aligning with Sutthiprapaporn et al.'s (2008) findings. However, we excluded such images and opted for MDCT datasets that facilitated clear PR identification. On the other hand, diagnosis of NPC is commonly performed in ENT clinics, utilizing symptom evaluation, physical examination, biopsy analysis, and MRI or MDCT imaging for accurate assessment (13). While CBCT imaging is predominantly used in dentistry, it is not practical for the diagnosis NPC. Therefore, our study employed MDCT images which are routinely utilized in ENT clinics.

Several studies have explored the detailed understanding of the PR and parapharyngeal space by analyzing images obtained from CBCT and MDCT (4,9,17-21). Loh et al. (1991) examined the PR morphometry in MDCT images of supine patients and reported a maximum PR depth of 18.8 mm (19). In contrast, Sutthiprapaporn et al. (2008) compared CBCT and MDCT techniques and found significantly lower PR depth values in CBCT imaging (1.1 mm on the left side, 2.1 mm on the right side) compared to their MDCT imaging results (6.8 mm on the left side, 9.8 mm on the right side) (9). Takasugi et al. (2016) evaluated CT images and reported a PR depth of 14 mm in the Japanese population (21). Furthermore, in two distinct investigations scrutinizing the Anatolian populace, Erdem et al. (2020) documented PR depths of 10.3 mm for males and 11.31 mm for females, while Kaplan et al. (2022) reported a variability spanning from 7.6 to 12 mm (4,18). In another CBCT study on an Anatolian sample, Serindere et al. (2022) reported PR depths of 5.26 mm on the left side and 5.54 mm on the right side (20). Our study revealed an average PR depth of 10.42 mm (male: 10.00 mm; female: 10.76 mm). These reported values of PR depths exhibit discrepancies both between different populations and within the same population.

The literature presents variations in the spatial relationship between the TL and the PNS. Interestingly, despite utilizing the same imaging modality and studying samples from either similar or different populations, divergent results have been documented. Furthermore, consensus is yet to be reached concerning the disparity between the left and right TL distances (4,9,20). Sutthiprapaporn et al. reported that both the torus tubarius and torus levatorius extend into the nasopharynx while in upright position. They additionally noted that these structures move downward when in supine position, leading to increased distances between the left and right sides (9). With the exception of the values reported by Sutthiprapaporn et al., previous studies have reported similar findings regarding the distance between the PNS and the PWN (4,9,20). The divergent outcomes in Sutthiprapaporn et al.'s study can likely be attributed to their notably smaller sample size. The same phenomenon of sample group discrepancy may also account for the lower values reported by Sutthiprapaporn et al. for the angle between the PR and sagittal axis (9).

The pharyngeal recesses (PRs) are classified into three distinct types based on their morphological characteristics. In our study, type 2 PRs were the most prevalent, followed by type 3 and type 1. Interestingly, similar pattern was observed in the study conducted by Takasugi et al., where type 2 PRs were also the most common, albeit with potentially different frequencies (21). On the other hand, Kaplan et al. reported in 2019 that type 1 PRs were the most prevalent, followed by type 3 and type 2, while their subsequent investigation in 2022 reported an altered order of type 3, type 2, and type 1 (17,18). These variations in the prevalence and ordering of PR types observed across different studies highlight the need for further exploration and elucidation of the underlying factors contributing to these discrepancies.

CONCLUSION

The reported discrepancies of reported measurements between different populations or even within the same population can be attributed to variations in imaging techniques, patient positioning, population-specific anatomical differences, and variations in sample sizes and demographics. A thorough understanding of these factors is crucial for accurate interpretation and clinical application of morphometric knowledge involving such anatomical regions. The technique which we employed, offers several advantages in understanding the anatomical features of the region. Utilization of 3D models reconstructed from MDCT datasets provided a comprehensive and high-resolution approach. This technique allows for a detailed visualization and analysis of the PR, offering a three-dimensional perspective that enhances our understanding of its morphometry and spatial relationships. The high-resolution imaging provided by MDCT datasets may contribute to a more accurate depiction of the PR and enable a better assessment of its variability across different populations. Furthermore, the capability to rotate the 3D models in desired spatial planes and the ability to accurately position radiological planes at specific landmarks confers practicality in conducting measurements. These measurements would otherwise be challenging through conventional morphometric analysis methodologies. Therefore, our study highlights the potential benefits of using 3D models generated from MDCT datasets to further explore and elucidate the morphometric characteristics of the PR, advancing our understanding of this anatomical region.

This study has several limitations. Firstly, the analysis was based on MDCT datasets obtained from a single center, limiting the ethnic diversity of the sample and potentially affecting the generalizability of the findings to other populations. Secondly, comparisons with other studies in the literature were primarily performed

with CBCT images, rather than 3D models. Differences in imaging modalities may introduce variations in measurements and hinder direct result comparisons. Furthermore, the sample size of 97 MDCT DICOM datasets, while substantial, should be considered in the interpretation of the results. Lastly, this study focused solely on morphometric analysis and did not consider other relevant factors such as demographics, clinical data, or functional aspects. Future studies could address these limitations and adopt a multidimensional approach to enhance our understanding of the pharyngeal recess and parapharyngeal space.

Financial disclosures: *The authors declared that this study has received no financial support.*

Conflict of Interest: *The authors have no conflicts of interest to declare.*

Ethical approval: *Ethical approval was waived by the local Ethics Committee of Cukurova University due to the retrospective nature of the study and the utilization of routine care procedures (Protocol no: 7.4.23/132).*

REFERENCES

1. Mudry A. Pharyngeal recess or Rosenmuller's fossa: Its first description revisited. Head Neck. 2021;43:2295-6.
2. Amene C, Cosetti M, Ambekar S, et al. Johann Christian Rosenmuller (1771-1820): A historical perspective on the man behind the fossa. J Neurol Surg B Skull Base. 2013;74:187-93.
3. Chen YP, Chan ATC, Le QT, et al. Nasopharyngeal carcinoma. Lancet. 2019;394:64-80.
4. Erdem S, Zengin AZ, Erdem S. Evaluation of the pharyngeal recess with cone-beam computed tomography. Surg Radiol Anat. 2020;42:1307-13.
5. Mankowski NL, Bordoni B. Anatomy, head and neck, nasopharynx. Treasure Island (FL): StatPearls Publishing. https://www.ncbi.nlm.nih.gov/books/NBK557635/ access date 25.05.2023.
6. Tang Y, Bie X, Yu S, Sun X. Study of the anatomical structure of the nasopharyngeal cavity and distribution of the air flow field. J Craniofac Surg. 2020;31:1937-41.
7. King AD, Zee B, Yuen EH, et al. Nasopharyngeal cancers: Which method should be used to measure these irregularly shaped tumors on cross-sectional imaging? Int J Radiat Oncol Biol Phys. 2007;69:148-54.
8. Chen J, Luo J, He X, Zhu C. Evaluation of contrast-enhanced computed tomography (CT) and magnetic resonance imaging (MRI) in the detection of retropharyngeal lymph node metastases in nasopharyngeal carcinoma patients. Cancer Manag Res. 2020;12:1733-9.
9. Sutthiprapaporn P, Tanimoto K, Ohtsuka M, et al. Improved inspection of the lateral pharyngeal recess using cone-beam computed tomography in the upright position. Oral Radiol. 2008;24:71-5.
10. Erdem H, Cevik Y, Safak NK, et al. Morphometric analysis of the infratemporal fossa using three-dimensional (3D) digital models. Surg Radiol Anat. 2023;45:729-34.
11. Guo R, Mao YP, Tang LL, et al. The evolution of nasopharyngeal carcinoma staging. Br J Radiol. 2019;92:20190244.
12. Koo TK, Li MY. A guideline of selecting and reporting intraclass correlation coefficients for reliability research. J Chiropr Med. 2016;15:155-63.
13. Tang LL, Chen YP, Chen CB, et al. The chinese society of clinical oncology (CSCO) clinical guidelines for the diagnosis and treatment of nasopharyngeal carcinoma. Cancer Commun (Lond). 2021;41:1195-227.
14. Jacobs R, Salmon B, Codari M, et al. Cone beam computed tomography in implant dentistry: recommendations for clinical use. BMC Oral Health. 2018;18:88.
15. MacDonald D. Cone-beam computed tomography and the dentist. J Investig Clin Dent. 2017;8:10.
16. Sutthiprapaporn P, Tanimoto K, Ohtsuka M, et al. Positional changes of oropharyngeal structures due to gravity in the upright and supine positions. Dentomaxillofac Radiol. 2008;37:130-5.
17. Kaplan FA, Bayrakdar IS, Bilgir E. Evaluation of rosenmuller fossa with cone beam computed tomography: A retrospective radio-anatomical study. Selcuk Dent J. 2019;6:195-9.
18. Kaplan FA, Saglam H, Bilgir E, et al. Radiological evaluation of the recesses on the posterior wall of the nasopharynx with cone-beam computed tomography. Niger J Clin Pract. 2022;25:55-61.
19. Loh LE, Chee TS, John AB. The anatomy of the fossa of rosenmuller: Its possible influence on the detection of occult nasopharyngeal carcinoma. Singapore Med J. 1991;32:154-5.
20. Serindere G, Gunduz K, Avsever H, Orhan K. The anatomical and measurement study of rosenmuller fossa and oropharyngeal structures using cone beam computed tomography. Acta Clin Croat. 2022;61:177-84.
21. Takasugi Y, Futagawa K, Konishi T, et al. Possible association between successful intubation via the right nostril and anatomical variations of the nasopharynx during nasotracheal intubation: A multiplanar imaging study. J Anesth. 2016;30:987-93.